

Polymer Chemistry

Accepted Manuscript



This is an *Accepted Manuscript*, which has been through the Royal Society of Chemistry peer review process and has been accepted for publication.

Accepted Manuscripts are published online shortly after acceptance, before technical editing, formatting and proof reading. Using this free service, authors can make their results available to the community, in citable form, before we publish the edited article. We will replace this *Accepted Manuscript* with the edited and formatted *Advance Article* as soon as it is available.

You can find more information about *Accepted Manuscripts* in the [Information for Authors](#).

Please note that technical editing may introduce minor changes to the text and/or graphics, which may alter content. The journal's standard [Terms & Conditions](#) and the [Ethical guidelines](#) still apply. In no event shall the Royal Society of Chemistry be held responsible for any errors or omissions in this *Accepted Manuscript* or any consequences arising from the use of any information it contains.



Journal Name

ARTICLE

Pyridine-bridged diketopyrrolopyrrole conjugated polymers for field-effect transistors and polymer solar cells

Received 00th January 20xx,
Accepted 00th January 20xx

DOI: 10.1039/x0xx00000x

www.rsc.org/

Xiaotao Zhang,^a Chengyi Xiao,^a Andong Zhang,^a Fangxu Yang,^a Huanli Dong,^a Zhaohui Wang,^a Xiaowei Zhan,^b Weiwei Li^{*a} and Wenping Hu^{*a,c}

Five wide or medium band gap diketopyrrolopyrrole (DPP) – based conjugated polymers with pyridine as bridges were developed for organic field-effect transistors (OFETs) and polymer solar cells (PSCs). By introducing copolymerized aromatic building blocks from strong electron-donating units to electron-deficient units into conjugated backbone, the highest occupied molecular orbital (HOMO) and lowest unoccupied molecular orbital (LUMO) levels of the DPP polymers were tailored to the low-lying position. Therefore, the polarity of charge transport in OFETs can be switched from p-type to n-type. The DPP polymer with the low-lying LUMO of -3.80 eV provides hole-only mobility of $2.95 \times 10^{-2} \text{ cm}^2 \text{ V}^{-1} \text{ s}^{-1}$, while electron-only mobility of $1.24 \times 10^{-3} \text{ cm}^2 \text{ V}^{-1} \text{ s}^{-1}$ is found in the DPP polymer with LUMO of -4.22 eV. Further investigation of photovoltaic cells based on these DPP polymers show modest power conversion efficiency (PCE) around 2%. Our results demonstrate that wide band gap pyridine-bridged DPP polymers have potential application in OFETs and OSCs by adjusting their energy level with alternated units on the conjugated backbone.

Introduction

Diketopyrrolopyrrole (DPP) based conjugated polymers have been intensively investigated for organic electronics, such as organic field-effect transistors (OFETs)¹ and polymer solar cells (PSCs)² since 2008.³ DPP derivatives were prepared from aromatic nitriles with succinic acid diesters,⁴ where aromatic units as bridge have the crucial influence on the properties of DPP polymers. Thienyl-bridged DPP polymers are mostly reported, with high hole⁵⁻⁸ and electron mobility⁹ above $1 \text{ cm}^2 \text{ V}^{-1} \text{ s}^{-1}$ in OFETs and PCE up to 8% in PSCs.^{10,11} Analogy of thiophene, such as thienothiophene,¹¹⁻¹³ selenophene,^{14,15} furan¹⁶⁻¹⁸ and thiazole,^{19,20} were also applied as bridges for DPP polymers to show promising performance in OFETs and PSCs. Electron donating thiophene and its analogy as bridge combined with strong electron deficient DPP core easily provide DPP polymers near-infrared absorption up to 1000 nm,¹⁴ which is especially beneficial for tandem and multi-junction solar cells.²¹⁻²⁴ In another aspect, DPP polymers desire excellent crystallinity and high charge carrier mobilities

that make them interesting to be explored as wide band gap polymers for OFETs and PSCs, but relative polymers are rarely studied.²⁵⁻²⁷

Conjugated polymers alternated with electron donor and acceptor are widely reported toward tunable absorption spectra and energy level via internal charge transfer.²⁸ DPP core with strong electron deficient ability requires weak donating units to form wide band gap polymer. When thienyl-bridged DPP polymers copolymerized with weak donors, such as biphenyl units,²⁶ carbazole^{29,30} and fluorene³¹⁻³³ derivatives, absorption onset of DPP polymers can be tuned to around 750 nm. Further blue-shifted absorption spectra to visible region for DPP polymers desire the modification of bridges with weak donating ability compared to thiophene. Phenyl-bridged DPP polymers as wide band gap materials are widely reported for application of pigment,³⁴ photo- or electron-luminescence,^{35,36} but showing poor performance in OFETs³⁷ and PSCs (lower than 2%).²⁵⁻³⁹ The dihedral angle between phenyl unit and DPP core around 30° makes the twist conjugated backbone of DPP polymers that will influence the crystallinity and charge transport.⁴⁰

The dihedral angle of phenyl-bridged DPP units originated from adjacent H atom on phenyl unit and methyl group attached to amide of DPP core, which can be eliminated via replacing of benzene by pyridine.²⁷ Wide band gap DPP polymers can be made with pyridine as bridge due to its similar donating ability with benzene. In addition, electron-withdrawing amine group (C=N) at pyridine unit also helps DPP

^a Beijing National Laboratory for Molecular Sciences, CAS Key Laboratory of Organic Solids, Institute of Chemistry, Chinese Academy of Sciences, Beijing 100190, P. R. China. E-mail: liweiwei@iccas.ac.cn or huwp@iccas.ac.cn

^b Department of Materials Science and Engineering, College of Engineering, Peking University, Beijing 100871, China

^c Collaborative Innovation Center of Chemical Science and Engineering (Tianjin) & Department of Chemistry, School of Science, Tianjin University, Tianjin 300072, China

† Electronic Supplementary Information (ESI) available: [details of any supplementary information available should be included here]. See DOI: 10.1039/x0xx00000x

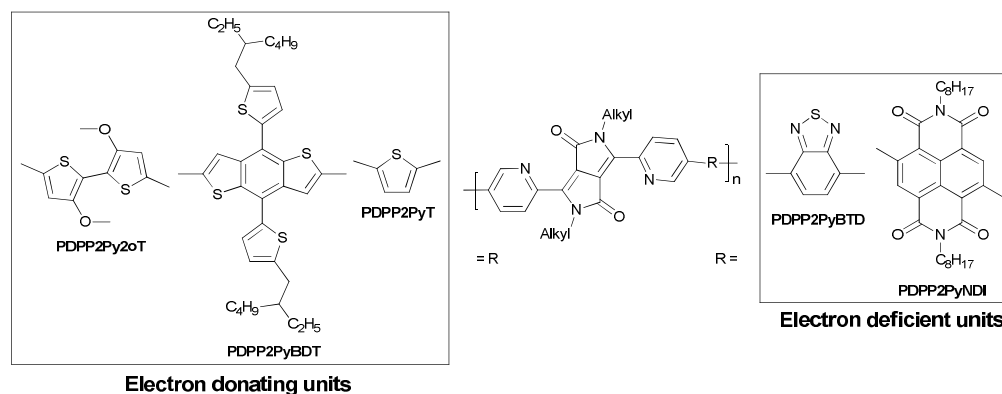


Fig. 1 Chemical structures of pyridine-bridged DPP polymers. Alkyl = octyldodecyl (OD) for PDPP2Py2oT and Alkyl = hexyldecyl (HD) for other polymers.

polymers to achieve deep highest occupied molecular orbital (HOMO) and lowest unoccupied molecular orbital (LUMO) levels that are especially beneficial for high open circuit voltage (V_{oc}) in PSCs. Pyridine-bridged DPP polymers have been reported for high electron mobilities of $6.3 \text{ cm}^2 \text{ V}^{-1} \text{ s}^{-1}$ for OFETs⁴¹ and PSCs with PCE of 4.9%.²⁷ It will be useful to further explore the pyridine-bridged DPP polymers for application in OFETs and PSCs.

In this work, we systematically design and synthesis a series of pyridine-bridged DPP polymers alternating with a variety of different aromatic units (Fig. 1). All the polymers have wide or medium band gap (1.41 – 1.85 eV), and their HOMO and LUMO levels were increased following by reducing electron donating ability or increasing electron withdrawing ability of alternated aromatic units. PDPP2Py2oT with strong donating dimethoxy-bithiophene (2oT) has low LUMO and HOMO levels of -3.87 eV and -5.28 eV, performing p-type OFETs. When using weak donor such as benzodithiophene (BDT) and thiophene (T), PDPP2PyBDT and PDPP2PyT show ambipolar OFETs. Further increasing HOMO and LUMO levels can be realized by introducing electron withdrawing benzothiadiazole (BTD) and naphthadiimide (NDI) into DPP polymers. PDPP2PyNDI has the deepest LUMO and HOMO levels (-4.22 eV and -6.07 eV) with n-type OFETs. Pyridine-bridged DPP polymers were also applied in PSCs with PCE up to 2.4%. We demonstrate that by modifying the molecular polarity of copolymerized units on conjugated backbone of DPP polymers, the energy level and polarity of charge transport can be varied and hence influence their properties in OFETs and PSCs.

Experimental

Materials and Measurements

All synthetic procedures were performed under nitrogen (N_2) atmosphere. Commercial chemicals were used as received. THF and Toluene were distilled from sodium under N_2 atmosphere and benzophenone was acted as the indicator. [6,6]-phenyl-C71-butyric acid methyl ester ([70]PCBM) was

purchased from Solenne BV. The monomer 4,9-dibromo-2,7-dioctylbenzo[*lmn*][3,8]phenanthroline-1,3,6,8(2*H*,7*H*)-tetraone, (4,8-bis(5-(2-ethylhexyl)thiophen-2-yl)benzo[1,2-*b*:4,5-*b'*]dithiophene-2,6-diyl)bis(trimethylstannane) (4), 2,5-bis(trimethylstannyl)thiophene (5) and 4,7-bis(4,4,5,5-tetramethyl-1,3,2-dioxaborolan-2-yl)benzo[*c*][1,2,5]thiadiazole (6) were purchased from Sunatech Inc. and recrystallized for polymerization.

3,6-bis(5-bromopyridin-2-yl)-2,5-bis(2-octyldodecyl)pyrrolo[3,4-*c*]pyrrole-1,4(2*H*,5*H*)-dione (1),²⁷ and (3,3'-dimethoxy-[2,2'-bithiophene]-5,5'-diyl)bis(trimethylstannane) (2)⁴² were synthesized according to literature procedures.

¹H-NMR and ¹³C-NMR spectra were recorded at 400 MHz and 100 MHz on a Bruker ANACE spectrometer with CDCl_3 as the solvent and tetramethylsilane (TMS) as the internal standard. Molecular weight of DPP polymers was determined with GPC at 140 °C on a PL-GPC 220 system using a PL-GEL 10 μm MIXED-B column and *ortho*-dichlorobenzene (*o*-DCB) as the eluent against polystyrene standards. Low concentration of 0.1 mg mL^{-1} polymer in *o*-DCB was applied to reduce aggregation. Electronic spectra were recorded on a JASCO V-570 spectrometer. Cyclic voltammetry was performed under an inert atmosphere with a scan rate of 0.1 V s^{-1} and 1 M tetrabutylammonium hexafluorophosphate in *o*-DCB as the electrolyte. The working, counter and reference electrodes were glassy carbon, Pt wire and Ag/AgCl, respectively. The concentration of the sample in the electrolyte was approximately 1 mM, based on monomers. All potentials were corrected against Fc/Fc^+ . X-Ray diffraction (XRD) measurements were obtained in reflection mode at 40 kV and 200 mA with Cu $\text{K}\alpha$ radiation using a 2-kW Rigaku D/max-2500 X-ray diffractometer. Grazing incidence wide-angle X-ray scattering (GIWAXS) experiments were conducted at XEUSS SAXS/WAXS equipment. Density function theory (DFT) calculations were performed at the B3LYP/6-31G* level of theory by using the Gaussian 09 program package. Atom force microscope (AFM) images of films were obtained by using a Digital Instruments Nanoscope IIIa Multimode atomic force microscope in tapping mode.

Organic field-effect transistors were fabricated using heavily doped silicon wafers as the common gate electrode with a 300

nm thermally oxidized SiO₂ layer which was modified by OTS as gate dielectric. Electrodes of Au (25 nm) were vacuum deposited first and then polymer thin films were spin coated on the substrate from *o*-DCB or chloroform solution with thickness around 30 – 50 nm, and then moved into glovebox filled with N₂. After thermal annealing at corresponding temperature, the devices were measured on an Agilent B1500 semiconductor parameter analyzer at room temperature.

Photovoltaic devices were made by spin coating poly-(ethylenedioxythiophene):poly(styrene sulfonate) (PEDOT:PSS) (Clevios P, VP Al 4083) onto precleaned, patterned indium tin oxide (ITO) substrates (15 Ω per square). The photoactive layer was deposited by spin coating a chloroform solution containing the polymers and [70]PCBM with 1:2 (w/w) ratio and the appropriate amount of 1,8-diiodooctane (DIO), 1-chloronaphthalene (1-CN) or *o*-DCB. Ca (20 nm) and Al (100 nm) were deposited by vacuum evaporation at $\sim 1 \times 10^{-5}$ Pa as the back electrode. The active area of the cells was 0.04 cm². An XES-70S1 (SAN-EI electric Co., Ltd.) solar simulator (AAA grade, 70 × 70 mm² photobeam size) coupled with AM 1.5 G solar spectrum filters was used as the light source, and the optical power at the sample was 100 mW cm⁻². A 2 × 2 cm² monocrystalline silicon reference cells (SRC-1000-TC-QZ) was purchased from VLSI standards Inc. The current-voltage (*I*-*V*) measurement of the devices was conducted using a computer-controlled Agilent B2912A Precision Source/Measure Unit. The external quantum efficiency (EQE) spectrum was measured using a Solar Cell Spectral Response Measurement System QE-R3011 (Enlitech Co., Ltd.). The light intensity at each wavelength was calibrated using a standard single crystal Si photovoltaic cell.

3,6-bis(5-bromopyridin-2-yl)-2,5-bis(2-hexyldecyl)pyrrolo[3,4-c]pyrrole-1,4(2H,5H)-dione (**3**)

To a degassed solution of 3,6-bis(5-bromopyridin-2-yl)pyrrolo[3,4-c]pyrrole-1,4(2H,5H)-dione²⁷ (1.99 g, 4.44 mmol) in N, N-dimethylformamide (50 mL), anhydrous potassium carbonate (1.85 g, 13.4 mmol) was added and heated under argon protection. 2-hexyldecyl bromide (4.08 g, 13.4 mmol) was injected in one portion by syringe. After the reaction was stirred for 12 h at 140 °C, the solution was cooled to room temperature, poured into 500 mL of ice water, and then extracted with CH₂Cl₂. After being dried in a vacuum, the crude product was purified by silica gel chromatography using dichloromethane as eluent to obtain a red solid powder (1.4 g, 35%). ¹H NMR (400 MHz, CDCl₃) δ 8.92 (d, 2H), 8.74 (d, 2H), 8.01 (dd, 2H), 4.28 (d, 4H), 1.60 (s, 2H), 1.22 (d, 54H), 0.85 (dd, 12H). ¹³C NMR (100 MHz, CDCl₃) δ 162.77, 150.40, 146.34, 145.27, 139.99, 128.74, 122.87, 111.71, 46.55, 38.50, 32.19, 32.10, 31.72, 30.29, 29.96, 29.84, 29.61, 26.61, 22.96, 14.40. MS (MALDI): calculated: 896.92, found: 896.9 (M⁺). Anal. Calcd. for C₄₈H₇₂Br₂N₄O₂: C, 64.28; H, 8.09; N, 6.25. Found: C, 64.46; H, 8.07; N, 6.14.

2,7-dioctyl-4,9-bis(tributylstannyl)benzo[*lmn*][3,8]phenanthroline-1,3,6,8(2H,7H)-tetraone (**7**)

A solution of 4,9-dibromo-2,7-dioctylbenzo[*lmn*][3,8]phenanthroline-1,3,6,8(2H,7H)-tetraone (0.500 g, 0.77 mmol), hexabutylstannane (1.00 g, 1.73 mmol), and tri-*o*-tolylphosphine (0.051 g, 0.169 mmol) in toluene (10 mL) was deoxygenated with N₂. Tris(dibenzylideneacetone)dipalladium (Pd₂(dba)₃) (0.039 g, 0.042 mmol) was added and the reaction was heated to 90 °C overnight. Additional portions of tri-*o*-tolylphosphine (0.051 g, 0.169 mmol) and Pd₂(dba)₃ (0.039 g, 0.042 mmol) were added and the reaction was stirred at 90 °C for an additional 2 d. After cooling, the reaction mixture was filtered through a plug of silica gel eluting with dichloromethane/petroleum ether (1:2) and the solvent was removed under reduced pressure. The crude product was recrystallized from methanol to yield a light yellow solid (0.180 g, 22%). ¹H NMR (400 MHz, CDCl₃) δ 8.95 (s, 2H), 4.27-4.12 (m, 4H), 1.78-1.61 (m, 4H), 1.62-1.48 (m, 12H), 1.46-1.18 (m, 44H), 0.87 (t, J=7.3 Hz, 24H). ¹³C NMR (100 MHz, CDCl₃) δ 164.12 (s), 138.35 (s), 132.16 (s), 41.24 (s), 32.13 (s), 29.54 (t, J=8.9 Hz), 28.43 (s), 27.71 (s), 27.35 (s), 22.93 (s), 14.37 (s), 14.01 (s), 11.86 (s). Anal. Calcd. for C₅₄H₉₀N₂O₄Sn₂: C, 60.69; H, 8.49; N, 2.62. Found: C, 61.01; H, 8.46; N, 2.69.

PDPP2Py2oT

To a degassed solution of monomer **1** (211.87 mg, 0.21 mmol), (3, 3'-dimethoxy-[2, 2'-bithiophene]-5,5'-diyl)bis(trimethylstannane) (**2**) (115.87 mg, 0.21 mmol) in toluene (4 mL) and DMF (0.4 mL), Pd₂(dba)₃ (5.77 mg, 6.3 μmol) and triphenylphosphine (PPh₃) (6.61 mg, 25.2 μmol) were added. The mixture was stirred at 115 °C for 24 h, after which it was precipitated in methanol and filter through a Soxhlet thimble. The polymer was extracted with acetone, hexane, dichloromethane and chloroform. The chloroform fraction was reduced and the polymer was precipitated in acetone. The polymer was collected by filtering over a 0.45 μm PTFE membrane filter and dried in a vacuum oven to yield PDPP2Py2oT (160 mg, 71%) as a dark solid. GPC (*o*-DCB, 140 °C): *M*_n = 9.9 kg mol⁻¹, PDI = 6.63. Anal. Calcd. for C₆₆H₉₆N₄O₄S₂: C, 73.83; H, 9.01; N, 5.22. Found: C, 72.81; H, 8.86; N, 5.10.

PDPP2PyBDT

Same procedure as for PDPP2Py2oT was used, but now **3** (159.31 mg, 0.18 mmol) and (4,8-bis(5-(2-ethylhexyl)thiophen-2-yl)benzo[1,2-*b*:4,5-*b'*]dithiophene-2,6-diyl)bis(trimethylstannane) (**4**) (160.74 mg, 0.18 mmol) were used as the monomers. Yield: 98.2 mg, 42%. GPC (*o*-DCB, 140 °C): *M*_n = 24.1 kg mol⁻¹, PDI = 3.13. Anal. Calcd. for C₈₂H₁₁₂N₄O₂S₄: C, 74.95; H, 8.59; N, 4.26. Found: C, 74.40; H, 8.65; N, 4.19.

PDPP2PyT

Same procedure as for PDPP2Py2oT was used, but now **3** (193.62 mg, 0.22 mmol) and **2**, 5-bis(trimethylstannyl)thiophene (**5**) (88.35 mg, 0.22 mmol) were used as the monomers. Yield: 124.5 mg (70%). GPC (*o*-DCB, 140 °C): *M*_n = 24.5 kg mol⁻¹, PDI = 2.75. Anal. Calcd. for C₅₂H₇₄N₄O₂S: C, 76.24; H, 9.10; N, 6.84. Found: C, 75.78; H, 8.95; N, 6.73.

PDPP2PyBDT

To a degassed solution of monomer **3** (143.88 mg, 0.016 mmol), 4,7-bis(4,4,5,5-tetramethyl-1,3,2-dioxaborolan-2-yl)benzo[*c*][1,2,5]thiadiazole (**6**) (62.29 mg, 0.16 mmol) in H₂O (0.5 mL) and toluene (5 mL) containing 2 M K₂CO₃, Tetrakis(triphenylphosphine)palladium(0) (Pd(PPh₃)₄) (10.75 mg, 9.3 μmol) were added. The mixture was stirred at 80 °C for 24 h, after which it was precipitated in methanol, washed by water, and filtered through a Soxhlet thimble. The polymer was extracted with acetone, hexane, and chloroform. The chloroform fraction was reduced and the polymer was precipitated in acetone. The polymer was collected by filtering over a 0.45 μm PTFE membrane filter and dried in a vacuum oven to yield PDPP2PyBTD (57 mg, 41%) as a dark solid. GPC (*o*-DCB, 140 °C): *M_n* = 6.1 kg mol⁻¹, PDI = 2.49. Anal. Calcd. for C₅₄H₇₄N₆O₂S: C, 74.44; H, 8.56; N, 9.65. Found: C, 71.60; H, 8.48; N, 8.99.

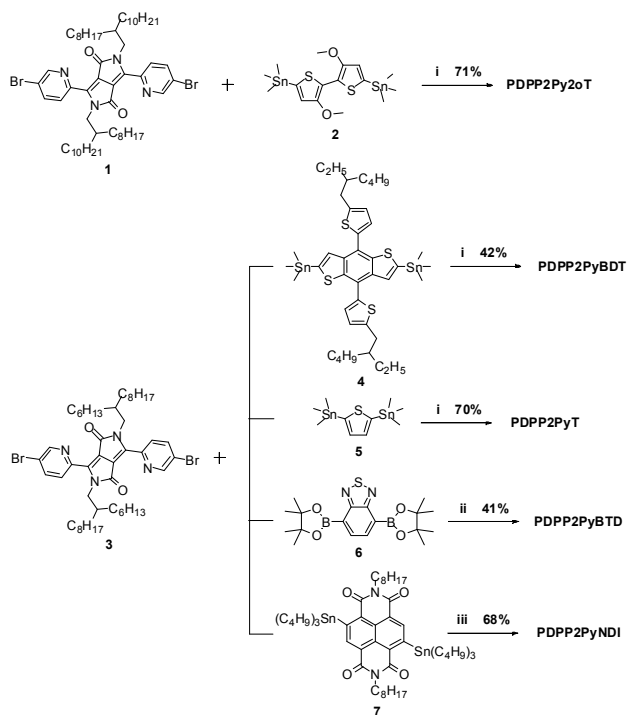
PDPP2PyNDI

To a degassed solution of monomer **3** (100 mg, 0.11 mmol), **7** (119 mg, 0.11 mmol) in toluene (3 mL) and DMF (0.3 mL), Pd₂(dba)₃ (3.02 mg, 3.3 μmol), PPh₃ (3.46 mg, 13.2 μmol) and CuI (4.19 mg, 22 μmol) were added. The mixture was stirred at 115 °C for 24 h, after which it was precipitated in methanol and filter through a Soxhlet thimble. The polymer was extracted with acetone and hexane. The polymer was dissolved in chloroform and then precipitated in acetone. The polymer was collected by filtering over a 0.45 μm PTFE membrane filter and dried in a vacuum oven to yield PDPP2PyNDI (93 mg, 68%) as a dark solid. GPC (*o*-DCB, 140 °C): *M_n* = 15.2 kg mol⁻¹, PDI = 2.39. Anal. Calcd. for C₇₈H₁₀₈N₆O₆: C, 76.43; H, 8.88; N, 6.86. Found: C, 76.05; H, 9.13; N, 6.17.

Results and discussion

Synthesis

The route for pyridine-bridged DPP polymers is shown in Scheme 1. PDPP2Py2oT was prepared by Stille polymerization with bis(bromopyridinyl)-DPP monomer and bisstannyl-bismethoxy-bithiophene (2oT) monomer. Octyldodecyl (OD) side chains were applied to provide enough solubility for the polymer. A catalyst system based on Pd₂(dba)₃ as source of palladium with PPh₃ as ligand combined with reaction solvent of toluene/DMF were used to achieve optimized molecular weight. PDPP2PyBDT with benzodithiophene (BDT) and PDPP2PyT with thiophene (T) were also made via Stille polymerization with similar condition as PDPP2Py2oT. For PDPP2PyNDI with electron withdrawing naphthadiimide (NDI), CuI was added into Stille polymerization to get high molecular weight.⁴³ We observed that the polymerization would not progress if lacking of CuI. PDPP2PyBDT was polymerized by Suzuki polycondensation with Pd(PPh₃)₄ as catalyst under 80 °C. The molecular weight of DPP polymers was determined by gel permeation chromatography (GPC) using *o*-dichlorobenzene (*o*-DCB) as eluent. The GPC column was held at 140 °C and the



Scheme 1 Synthesis route of pyridine-bridged DPP polymers. (i) Stille polymerization by using Pd₂(dba)₃/PPh₃ in toluene/DMF (10:1, v/v) at 115 °C. (ii) Suzuki polymerization by using Pd(PPh₃)₄/K₂CO₃ (aq)/Aliquat 336 in toluene at 80 °C. (iii) Stille polymerization by using Pd₂(dba)₃/PPh₃/CuI in toluene/DMF (10:1, v/v) at 115 °C.

polymer concentration was 0.1 mg/ml to reduce aggregation of polymers. These polymers perform the weight-average molecular weight (*M_w*) of 15.1 – 75.4 kg mol⁻¹ but with high polydispersity index (PDI) of 2.39 – 6.63 (Table 1), so the number molecular weight (*M_n*) is modest (6.1 – 24.5 kg mol⁻¹). As shown in Fig. S1 (ESI⁺), low *M_n* and high PDI was quite different from thienyl-bridged DPP polymers.⁴⁴ This is probably due to the less reaction activity of dibromo-pyridine-bridged DPP monomers.

Optical and electrochemical properties

The DPP polymers show red-shifted absorption spectra in thin films (Fig. 2a) compared to that in chloroform solution (Table 1 and Fig. S2, ESI⁺), indicating aggregation. PDPP2Py2oT with strong donating 2oT units performed near-infrared absorption spectra with absorption onset at 880 nm and optical band gap (*E_g*) of 1.41 eV. Other pyridine-bridged DPP polymers show similar wide band gap with *E_g* of 1.75 eV – 1.85 eV. It is desired to mention that PDPP2PyBDT and PDPP2PyNDI with electron

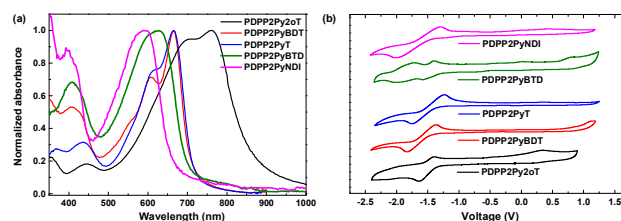
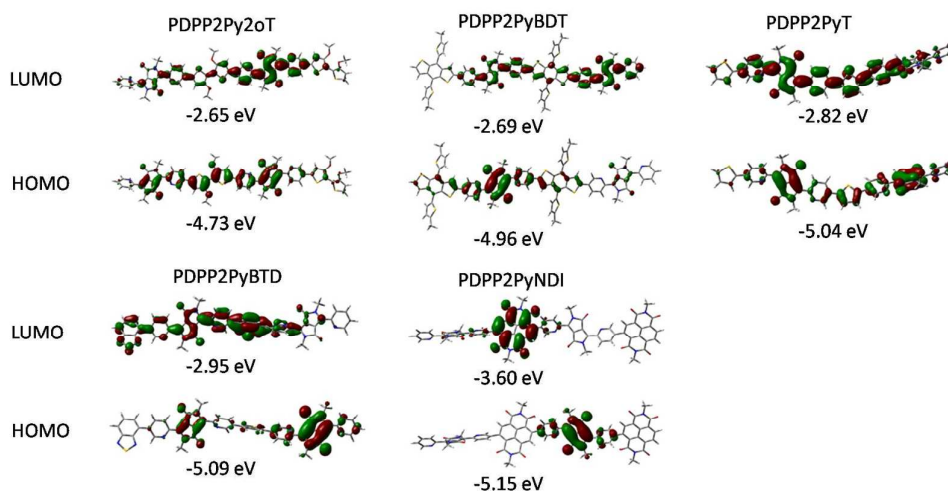


Fig. 2 (a) Optical absorption spectra of the polymers in solid state films and (b) cyclic voltammograms of the polymers in *o*-DCB. Potential vs. Fc/Fc⁺.

Table 1 Molecular weight, optical and electro-chemical properties of the pyridine-bridged DPP polymers.

Polymer	M_n^a (kg mol ⁻¹)	M_w^a (kg mol ⁻¹)	PDI	CHCl ₃ solution			Film		E_g^{film} (eV)	LUMO (eV) ^b	HOMO (eV) ^c
				λ_{peak} (nm)	λ_{onset} (nm)	E_g^{sol} (eV)	λ_{peak} (nm)	λ_{onset} (nm)			
PDPP2Py2oT	9.9	65.9	6.63	757	841	1.47	760	880	1.41	-3.80	-5.21
PDPP2PyBDT	24.1	75.4	3.13	665	690	1.80	665	708	1.75	-3.84	-5.59
PDPP2PyT	24.5	67.3	2.75	648	686	1.81	665	706	1.76	-3.89	-5.65
PDPP2PyBTD	6.1	15.1	2.49	585	663	1.87	628	704	1.76	-4.01	-5.77
PDPP2PyNDI	15.2	36.4	2.39	592	667	1.86	592	670	1.85	-4.22	-6.07

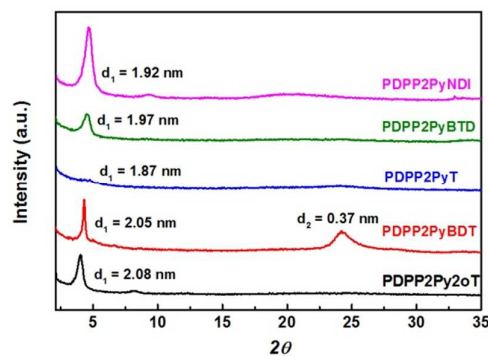
^aDetermined with GPC at 140 °C using *o*-DCB as the eluent. ^bDetermined using a work function value of -5.23 eV for Fc/Fc⁺. ^cDetermined as $E_{LUMO} - E_g^{film}$.

**Fig. 3** DFT frontier molecular orbitals for the segments of pyridine-bridged DPP polymers.

withdrawing BTD and NDI units show large band gap of 1.76 eV and 1.85 eV. As compare, their thienyl-bridged DPP polymers PDPP2TBT and PNDI-DPP have low band gap of 1.19 eV⁴⁵ and 1.15 eV.⁴⁶ This huge difference indicates the great influence of pyridine as bridge on their physical properties.

The energy levels of DPP polymers were determined using cyclic voltammetry in *o*-DCB solutions (Fig. 2b and Table 1). When electron donating ability decreased or electron withdrawing ability increased, DPP polymers show increased HOMO and LUMO levels. PDPP2Py2oT has LUMO and HOMO levels of -3.80 eV and -5.21 eV. The low HOMO level will help hole injection in OFETs but also reduce V_{oc} in PSCs. PDPP2PyBDT and PDPP2PyT with BDT and T as donor show similar LUMO level but high HOMO level that is beneficial for high V_{oc} in PSCs. PDPP2PyBTD with electron withdrawing BTD units provides LUMO level of -4.01 eV and HOMO level of -5.77 eV. Further increase of LUMO and HOMO level is realized by using NDI as building block, in which PDPP2PyNDI show LUMO level of -4.22 eV and IP of -6.07 eV. The LUMO and HOMO levels of PDPP2PyNDI are similar with fullerene derivative, indicating the potential application as non-fullerene electron acceptor for polymer-polymer solar cells. The great variation of energy level induced by copolymerized aromatic units would influence their electronic properties in OFETs and PSCs. Density functional theory (DFT) calculations on B3LYP/6-31G level were performed for extended oligomers based on these

DPP polymers. In the DFT calculations methyl units was used to replace of long alkyl chains in order to reduce the calculation time. Deep HOMO and LUMO levels were achieved from 2oT-based oligomer to NDI-based oligomer (Fig. 3), which has the similar trend as measured energy levels of DPP polymers. For PDPP2Py2oT, PDPP2PyBDT and PDPP2PyT with electron donating units, HOMO and LUMO orbitals are delocalized over the conjugated backbone. However, the HOMO orbitals of PDPP2PyBTD and PDPP2PyNDI are mainly delocalized over the DPP core and the LUMO orbitals are mainly delocalized over the BTD or NDI units. The dihedral angle between aromatic units and neighboring pyridine units is around 20° for

**Fig. 4** X-ray diffraction patterns of the DPP polymers thin films annealing at 150 °C for 10 min.

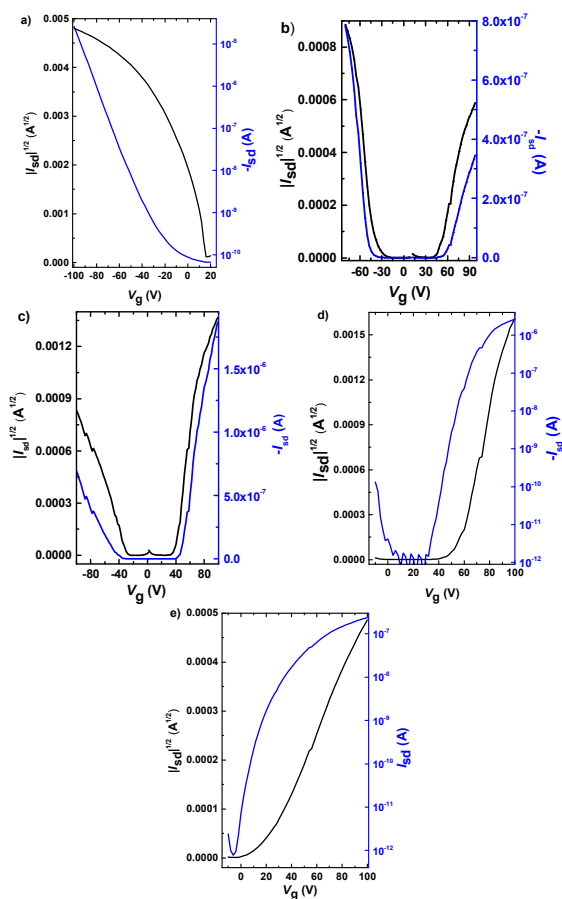


Fig. 5 Transfer characteristics for bottom-contact OFETs for the DPP polymers. (a) PDPP2Py2oT, (b) PDPP2PyBDT, (c) PDPP2PyT, (d) PDPP2PyBTD and (e) PDPP2PyNDI. W/L = 1400/50 μm , except for PDPP2PyBTD devices with W/L = 1400/10 μm .

Table 2 Field effect hole and electron mobility of the DPP polymers.

Polymer	Annealing Temperature ^a (°C)	μ_h ($\text{cm}^2 \text{V}^{-1} \text{s}^{-1}$)	μ_e ($\text{cm}^2 \text{V}^{-1} \text{s}^{-1}$)
PDPP2Py2oT	100	2.95×10^{-2}	-
PDPP2PyBDT	160	2.60×10^{-2}	2.67×10^{-3}
PDPP2PyT	100	1.65×10^{-3}	1.34×10^{-2}
PDPP2PyBTD	100	-	4.62×10^{-3}
PDPP2PyNDI	200	-	1.24×10^{-3}

^aAnnealing in glove box filled with N_2 under the temperature for 10 min.

PDPP2Py2oT, PDPP2PyBDT and PDPP2PyT. The dihedral angle was greatly increased to 38.20° for PDPP2PyBTD and 59.33° for PDPP2PyNDI (Fig. S3, ESI[†]).

Molecular stacking of DPP polymers was analyzed by X-ray diffraction (XRD) of the polymer thin films (Fig. 4 and Fig. S4, ESI[†]). All the pure polymer films drop casted from chloroform solutions displayed diffraction peaks (Fig. S4, ESI[†]) and the intensity of these peaks are increased after thermal annealing of thin films at 150°C (Fig. 4). The polymers show strong (100) diffraction peaks at $2\theta = 4.25^\circ$ (PDPP2Py2oT), 4.31° (PDPP2PyBDT), 4.48° (PDPP2PyBTD) and 4.61° (PDPP2PyNDI). PDPP2PyT performed weak diffraction peaks at $2\theta = 4.71^\circ$. The lamellar d -spacings are 1.87 – 2.08 nm (Fig. 4). PDPP2PyBTD and PDPP2PyNDI showed large dihedral angle (38.20° and

59.33°) on conjugated backbone (Fig. S3, ESI[†]), but they still performed good crystallinity with d -spacings of 1.97 nm and 1.92 nm. PDPP2PyBDT also showed weak and broad peak (010) at the angle of 24.21° , corresponding to the π - π stacking distance of 0.37 nm. For the other polymers, the (010) peak is too weak to be observed. GIWAXS was also applied to investigate the crystal behaviour of the polymers in thin films (Fig. S5, ESI[†]), showing that most of the polymers perform the diffraction in small angle region (0.22 – 0.4 \AA) in the in-plane and out-of-plane direction that is corresponding to the stacking of alkyl side chains.

Charge carrier mobility

Charge carrier mobility of the DPP polymers was determined in a bottom gate-bottom contact FET configuration. Highly n -doped Si wafer with a SiO_2 layer which contained strip gold electrodes was passivated with octadecyltrichlorosilane (OTS) self-assembled monolayers. DPP polymers dissolved in chloroform or o -DCB were spin-coated on the substrates and moved into the glovebox with N_2 . After annealing at corresponding temperature, the devices were measured at room temperature. Representative transfer curves were shown in Fig. 5. The mobility (μ) in the saturated region and the threshold voltage (V_T) were calculated using the following equation:

$$I_{DS} = (W/2L) C_i \mu (V_G - V_T)^2$$

Where W and L are the channel width and length, respectively, C_i is the unit dimensional dielectric capacitance of gate insulator, μ is the field-effect mobility, and V_T is the threshold voltage.

All devices exhibit very high on/off ratios ($I_{on/off}$: $10^5 - 10^7$). V_T is around $-20 - -30$ V for hole mobilities and $20 - 60$ V for electron mobilities. PDPP2Py2oT only exhibit hole mobility (μ_h) of $2.95 \times 10^{-2} \text{ cm}^2 \text{V}^{-1} \text{s}^{-1}$. OFETs based on PDPP2PyBDT and PDPP2PyT with weak donating building block shown typical ambipolar transfer characteristics (Fig. 5b and c). PDPP2PyBDT exhibited higher μ_h of $2.60 \times 10^{-2} \text{ cm}^2 \text{V}^{-1} \text{s}^{-1}$ compared to its electron mobility (μ_e) of $2.67 \times 10^{-3} \text{ cm}^2 \text{V}^{-1} \text{s}^{-1}$. However, PDPP2PyT showed higher μ_e of $1.34 \times 10^{-2} \text{ cm}^2 \text{V}^{-1} \text{s}^{-1}$ than μ_h of $1.65 \times 10^{-3} \text{ cm}^2 \text{V}^{-1} \text{s}^{-1}$. The trend of increased electron mobility and reduced hole mobility was probably due to increased LUMO and HOMO level of DPP polymers. Deep LUMO level would help electron injection from the gold electrodes but deep HOMO level is not beneficial for hole injection. Further enhancement of LUMO and HOMO level for PDPP2PyBTD and PDPP2PyNDI provides the polymers only electron mobilities around $10^{-3} \text{ cm}^2 \text{V}^{-1} \text{s}^{-1}$. OFETs clearly showed that modification of polymers structures by introducing building blocks with different electron-donating or withdrawing abilities can effectively tune the energy level and hole or electron mobilities.

Photovoltaic properties

Pyridine-bridged DPP polymers as electron donor blended with [70]PCBM as electron acceptor were further applied into photovoltaic devices, sandwiched between the transparent ITO/PEDOT:PSS front and the reflecting Ca/Al back electrodes. The photoactive layers comprising of DPP polymers and [70]PCBM were carefully optimized with respect to ratio of

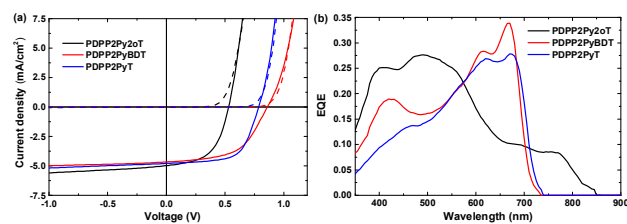


Fig. 6 (a) J - V characteristics in dark (dashed lines) and under white light illumination (solid lines) of optimized solar cells of the polymers with [70]PCBM. (b) EQE of the same devices.

Table 3 Solar cell parameters of optimized solar cells of the DPP polymers with [70]PCBM.

Polymer ^a	Thickness (nm)	J_{sc} (mA cm ⁻²)	V_{oc} (V)	FF	PCE (%)
PDPP2Py2oT	90	5.0	0.53	0.54	1.4
PDPP2PyBDT	100	4.7	0.86	0.55	2.2
PDPP2PyT	85	4.8	0.79	0.64	2.4

^aRatio of DPP-polymer to [70]PCBM is 1:2. Optimized spin coating solvent for active layer is CHCl₃ with 5% DIO as additive.

donor to acceptor, solvent with additive and layer thickness. PDPP2PyBDT and PDPP2PyNDI based cells have no photovoltaic effect due to their deep LUMO level, which induced low driving force for charge separation from donor to acceptor.

J - V characteristics of PDPP2Py2oT, PDPP2PyBDT and PDPP2PyT based cells were presented at Fig. 6 and the photovoltaic parameters were shown in Table 3. In general, photoactive layers based on DPP-polymer:[70]PCBM for optimized cells were spin coated from chloroform solution with 5% vol. 1,8-diiodooctane (DIO) as additive and the ratio of donor to acceptor is 1:2. When using 1-CN or *o*-DCB as additive, the solar cells provided lower PCEs (Table S1). PDPP2Py2oT with high-lying HOMO level provided low V_{oc} of 0.53 V, and PDPP2PyBDT and PDPP2PyT showed high V_{oc} of 0.86 V and 0.79 V due to their deep HOMO level. All these cells gave modest short circuit current density (J_{sc}) of 4.7 – 5.0 mA cm⁻², and fill factor of 0.54 – 0.64. Therefore, PCE based on DPP-polymer:[70]PCBM cells is 1.4% (PDPP2Py2oT), 2.2% (PDPP2PyBDT) and 2.4% (PDPP2PyT), which is much less than thienyl-bridged DPP polymers. Low PCE is mainly attributed to their low J_{sc} that also can be found from their external quantum efficiency (EQE) (Fig. 6b). PDPP2Py2oT:[70]PCBM cells showed low EQE (< 0.1) contributed from absorption of the polymer. PDPP2PyBDT and PDPP2PyT based cells also gave EQE lower than 0.35 in their absorption region. We also synthesized OD-PDPP2PyT with longer OD side chains so as to achieve high $M_n = 39.9$ kg mol⁻¹ and PDI = 3.76 compared to the polymer with HD units (Scheme S1), but the devices based on OD-PDPP2PyT provide very poor PCE of 0.43% (Table S2). The results confirm the previous observation that the DPP polymers with longer side chains yield low efficiency solar cells.⁴⁷

Low photon-conversion into electron efficiency based on these pyridine-bridged DPP polymers is desired to be discussed. It

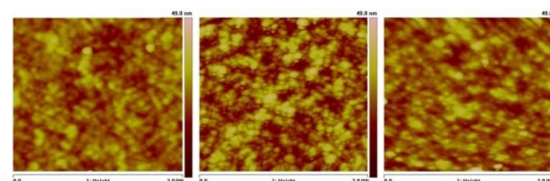


Fig. 7 AFM height image of optimized DPP-polymer:[70]PCBM (1:2) spin-coated from chloroform containing 5% vol. DIO. (a) PDPP2Py2oT, (b) PDPP2PyBDT and (c) PDPP2PyT. Root mean square (RMS) roughness is 3.3 nm, 5.02 nm and 3.81 nm from PDPP2Py2oT to PDPP2PyT.

has been reported that in thienyl-bridged DPP polymers based photovoltaic cells, energy loss ($E_{Loss} = E_g - eV_{oc}$) between band gap of donor polymer to V_{oc} has great influence on EQE of devices.²⁰ In these pyridine-bridged DPP polymer solar cells, E_{Loss} was calculated as 0.88 eV (PDPP2Py2oT), 0.89 eV (PDPP2PyBDT) and 0.97 eV (PDPP2PyT) that should be enough for exciton separation into free carriers. Poor EQE and PCE in these cells may originate from poor phase separation between polymer and [70]PCBM as shown in Fig. 7. In AFM height image of photoactive layers, large domain can be found in these polymer:[70]PCBM systems, indicating that exciton has the difficulty to diffusion into the interface of donor and acceptor. In addition, it should be also noted that, relatively low molecular weight of these pyridine-bridged DPP polymers indicate possible defect on the conjugated backbone, such as homo-coupling segment, which is detrimental to the photovoltaic device performance.⁴⁸ Further study based on optimization of polymerization condition to achieve high molecular weight of pyridine-bridged DPP polymers will be needed to improve the PCE of photovoltaic cells.

Conclusions

A series of conjugated polymers with DPP as core and pyridine as bridge were designed and synthesized, where alternated building blocks from electron donor to electron acceptor were introduced. Strong electron donating unit, such as bimethoxy-dithiophene, was incorporated into DPP polymers with low band gap of 1.41 eV. DPP polymers containing weak donor or electron acceptor as building blocks show wide band gap around 1.8 eV. The HOMO and LUMO levels of DPP polymers were influenced by incorporating building blocks, following the trends from strong donor to weak donor and electron acceptor. Therefore, polarity of charge transport in OFETs can be varied from p-type for PDPP2Py2oT with strong donor, to ambipolar behaviour for PDPP2PyBDT and PDPP2PyT alternated with weak donor, and n-type for DPP polymers with electron withdrawing units. Further investigation of photovoltaic devices based on these polymers showed modest PCE of 1.4 – 2.4% due to their low external quantum efficiency. The results show that energy level and charge transport properties of conjugated polymers, from hole-only to ambipolar and electron-only transport, can be effectively tuned via copolymerized building blocks. Further investigation on improving molecular weight is also needed for pyridine-

bridged DPP polymers toward high performance photovoltaic devices.

Acknowledgements

We thank Ralf Bovee and Prof. René A. J. Janssen at Eindhoven University of Technology (Tue, Netherlands) for GPC analysis, Dr. Jianqi Zhang at National Center for Nanoscience and Technology (Beijing, China) for GIWAXS measurement. This work was supported by the Recruitment Program of Global Youth Experts of China. The work was further supported by the Ministry of Science and Technology of China (2014CB643600, 2013CB933500), and the Strategic Priority Research Program (Grant No. XDB12030300) of the Chinese Academy of Sciences.

Notes and references

- C. B. Nielsen, M. Turbiez and I. McCulloch, *Adv. Mater.*, 2013, **25**, 1859-1880.
- X. Guo, A. Facchetti and T. J. Marks, *Chem. Rev.*, 2014, **114**, 8943-9021.
- M. M. Wienk, M. Turbiez, J. Gilot and R. A. J. Janssen, *Adv. Mater.*, 2008, **20**, 2556-2560.
- A. C. Rochat, L. Cassar and A. Iqbal, Euro Pat., 94911, 1983.
- I. Kang, T. K. An, J.-a. Hong, H.-J. Yun, R. Kim, D. S. Chung, C. E. Park, Y.-H. Kim and S.-K. Kwon, *Adv. Mater.*, 2013, **25**, 524-528.
- H. J. Chen, Y. L. Guo, G. Yu, Y. Zhao, J. Zhang, D. Gao, H. T. Liu and Y. Q. Liu, *Adv. Mater.*, 2012, **24**, 4618-4622.
- I. Kang, H.-J. Yun, D. S. Chung, S.-K. Kwon and Y.-H. Kim, *J. Am. Chem. Soc.*, 2013, **135**, 14896-14899.
- J. Y. Back, H. Yu, I. Song, I. Kang, H. Ahn, T. J. Shin, S.-K. Kwon, J. H. Oh and Y.-H. Kim, *Chem. Mater.*, 2015, **27**, 1732-1739.
- J. H. Park, E. H. Jung, J. W. Jung and W. H. Jo, *Adv. Mater.*, 2013, **25**, 2583-2588.
- K. H. Hendriks, G. H. L. Heintges, V. S. Gevaerts, M. M. Wienk and R. A. J. Janssen, *Angew. Chem., Int. Ed.*, 2013, **52**, 8341-8344.
- R. S. Ashraf, I. Meager, M. Nikolka, M. Kirkus, M. Planells, B. C. Schroeder, S. Holliday, M. Hurhangee, C. B. Nielsen, H. Sirringhaus and I. McCulloch, *J. Am. Chem. Soc.*, 2014, **137**, 1314-1321.
- H. Bronstein, Z. Chen, R. S. Ashraf, W. Zhang, J. Du, J. R. Durrant, P. Shakya Tuladhar, K. Song, S. E. Watkins, Y. Geerts, M. M. Wienk, R. A. J. Janssen, T. Anthopoulos, H. Sirringhaus, M. Heeney and I. McCulloch, *J. Am. Chem. Soc.*, 2011, **133**, 3272-3275.
- I. Meager, R. S. Ashraf, S. Mollinger, B. C. Schroeder, H. Bronstein, D. Beatrup, M. S. Vezie, T. Kirchartz, A. Salleo, J. Nelson and I. McCulloch, *J. Am. Chem. Soc.*, 2013, **135**, 11537-11540.
- K. H. Hendriks, W. Li, M. M. Wienk and R. A. J. Janssen, *J. Am. Chem. Soc.*, 2014, **136**, 12130-12136.
- L. Dou, W.-H. Chang, J. Gao, C.-C. Chen, J. You and Y. Yang, *Adv. Mater.*, 2013, **25**, 825-831.
- C. H. Woo, P. M. Beaujuge, T. W. Holcombe, O. P. Lee and J. M. J. Fréchet, *J. Am. Chem. Soc.*, 2010, **132**, 15547-15549.
- A. T. Yiu, P. M. Beaujuge, O. P. Lee, C. H. Woo, M. F. Toney and J. M. J. Fréchet, *J. Am. Chem. Soc.*, 2012, **134**, 2180-2185.
- L. T. Dou, J. Gao, E. Richard, J. B. You, C. C. Chen, K. C. Cha, Y. J. He, G. Li and Y. Yang, *J. Am. Chem. Soc.*, 2012, **134**, 10071-10079.
- B. Carsten, J. M. Szarko, L. Lu, H. J. Son, F. He, Y. Y. Botros, L. X. Chen and L. Yu, *Macromolecules*, 2012, **45**, 6390-6395.
- W. Li, K. H. Hendriks, A. Furlan, M. M. Wienk and R. A. J. Janssen, *J. Am. Chem. Soc.*, 2015, **137**, 2231-2234.
- L. T. Dou, J. B. You, J. Yang, C. C. Chen, Y. J. He, S. Murase, T. Moriarty, K. Emery, G. Li and Y. Yang, *Nat. Photon.*, 2012, **6**, 180-185.
- J. You, L. Dou, K. Yoshimura, T. Kato, K. Ohya, T. Moriarty, K. Emery, C.-C. Chen, J. Gao, G. Li and Y. Yang, *Nat Commun*, 2013, **4**, 1446.
- W. Li, A. Furlan, K. H. Hendriks, M. M. Wienk and R. A. J. Janssen, *J. Am. Chem. Soc.*, 2013, **135**, 5529-5532.
- O. Adebajo, P. P. Maharjan, P. Adhikary, M. Wang, S. Yang and Q. Qiao, *Energy Environ. Sci.*, 2013, **6**, 3150-3170.
- C. Kanimozhi, P. Balraju, G. D. Sharma and S. Patil, *J. Phys. Chem. B*, 2010, **114**, 3095-3103.
- W. Li, A. Furlan, W. S. C. Roelofs, K. H. Hendriks, G. W. P. van Pruissen, M. M. Wienk and R. A. J. Janssen, *Chem. Commun.*, 2014, **50**, 679-681.
- J. W. Jung, F. Liu, T. P. Russell and W. H. Jo, *Chem. Commun.*, 2013, **49**, 8495-8497.
- Y. J. Cheng, S. H. Yang and C. S. Hsu, *Chem. Rev.*, 2009, **109**, 5868-5923.
- Y. P. Zou, D. Gendron, R. Badrou-Aich, A. Najari, Y. Tao and M. Leclerc, *Macromolecules*, 2009, **42**, 2891-2894.
- J. Jo, D. Gendron, A. Najari, J. S. Moon, S. Cho, M. Leclerc and A. J. Heeger, *Appl. Phys. Lett.*, 2010, **97**, 203303-203303.
- E. Zhou, S. Yamakawa, K. Tajima, C. Yang and K. Hashimoto, *Chem. Mater.*, 2009, **21**, 4055-4061.
- L. Huo, J. Hou, H.-Y. Chen, S. Zhang, Y. Jiang, T. L. Chen and Y. Yang, *Macromolecules*, 2009, **42**, 6564-6571.
- A. P. Zoombelt, S. G. J. Mathijssen, M. G. R. Turbiez, M. M. Wienk and R. A. J. Janssen, *J. Mater. Chem.*, 2010, **20**, 2240-2246.
- G. Lange and B. Tieke, *Macromol. Chem. Physic.*, 1999, **200**, 106-112.
- T. Beyerlein and B. Tieke, *Macromol. Rapid. Comm.*, 2000, **21**, 182-189.
- T. Beyerlein, B. Tieke, S. Forero-Lenger and W. Brütting, *Syn. Met.*, 2002, **130**, 115-119.
- M.-F. Falzon, A. P. Zoombelt, M. M. Wienk and R. A. J. Janssen, *Phys. Chem. Chem. Phys.*, 2011, **13**, 8931-8939.
- W. Li, T. Lee, S. J. Oh and C. R. Kagan, *ACS Appl. Mater. Interfaces*, 2011, **3**, 3874-3883.
- L. Chen, D. Deng, Y. Nan, M. Shi, P. K. L. Chan and H. Chen, *J. Phys. Chem. C*, 2011, **115**, 11282-11292.
- C. Kim, J. Liu, J. Lin, A. B. Tamayo, B. Walker, G. Wu and T.-Q. Nguyen, *Chem. Mater.*, 2012, **24**, 1699-1709.
- B. Sun, W. Hong, Z. Yan, H. Aziz and Y. Li, *Adv. Mater.*, 2014, **26**, 2636-2642.
- T. H. Marks, A. Facchetti, US Pat., 8 859 714, 2014.
- L. E. Polander, A. S. Romanov, S. Barlow, D. K. Hwang, B. Kippelen, T. V. Timofeeva and S. R. Marder, *Org. Lett.*, 2012, **14**, 918-921.
- W. Li, K. H. Hendriks, A. Furlan, W. S. C. Roelofs, M. M. Wienk and R. A. J. Janssen, *J. Am. Chem. Soc.*, 2013, **135**, 18942-18948.
- W. Li, K. H. Hendriks, A. Furlan, A. Zhang, M. M. Wienk and R. A. J. Janssen, *Chem. Commun.*, 2015, **51**, 4290-4293.
- P. Wang, H. Li, C. Gu, H. Dong, Z. Xu and H. Fu, *Rsc Adv.*, 2015, **5**, 19520-19527.
- W. Li, K. H. Hendriks, A. Furlan, W. S. C. Roelofs, S. C. J. Meskers, M. M. Wienk and R. A. J. Janssen, *Adv. Mater.*, 2014, **26**, 1565-1570.
- K. H. Hendriks, W. Li, G. H. L. Heintges, G. W. P. van Pruissen, M. M. Wienk and R. A. J. Janssen, *J. Am. Chem. Soc.*, 2014, **136**, 11128-11133.